Jordan Journal of Civil Engineering, Volume **5**, No. **1**, **2011**

Assessing the Performance of Different Large Format Digital Cameras by Investigating the Geometric Accuracy and Camera Calibration

Khaldoun Qtaishat

Department of Civil and Environmental Engineering, Faculty of Engineering, Mu'tah University, Al-Karak, Jordan

ABSTRACT

This paper provides an independent investigation on the geometric accuracy and camera calibration of the new photogrammetric digital airborne camera systems, undertaken as a part of the German Society of Photogrammetry, Remote Sensing and Geoinfirmation (DGPF) project for investigating large format digital cameras (Vexcel Imaging UltraCamX, Z/I Imaging DMC and Z/I Imaging RMC Top 15). This paper presents results from the imaging data on 6 different flight days flown over a test site in Germany during a 10 week time window starting at the beginning of July till the middle of September 2008. Most of the sensors were flown at two different flying heights, resulting in two blocks with different Ground Sampling Distances (GSD); namely GSD 20cm and GSD 8cm.

In this paper, the digital camera calibration was assessed through analyzing and identifying any systematic patterns in the image residuals. A new calibration method was undertaken in this paper based on analyzing the systematic errors of the high and low flown residuals. The bundle adjustment will be re-computed based on the analysis of the systematic residual patterns. This approach is based on analyzing the systematic errors of the high flown residuals and re-computing the bundle adjustment of the low flown images based on the residual corrections of the high flown images. These corrections were computed from a block triangulation and applied because the systematic patterns were considered similar for all images.

The bundle adjustment will be re-computed based on the analysis of the systematic residual patterns. This approach is based on analyzing the systematic errors of the high flown residuals and re-computing the bundle adjustment of the low flown images based on the residual corrections of the high flown images.

The results introduced in this paper were significantly improved by using the traditional existing self-calibration method and the new calibration approach.

KEYWORDS: Large format digital camera, Interior calibration, Geometry.

INTRODUCTION

Nowadays, large format digital aerial cameras are increasingly replacing analogue aerial cameras. In some countries, analogue aerial cameras are even no longer accepted (Jacobsen, 2009). It was approximately 8 years ago when the first two commercial large format digital airborne cameras; DMC and ADS40, were launched at the Amsterdam ISPRS congress. The large format digital aerial cameras are now playing a significant role in the field of digital airborne imaging (Gruber et al., 2006). The geometric model of the sensing system should be determined to any block of images used for high precision measurement purposes in

Accepted for Publication on 15/1/2011.

photogrammetry (Cramer, 2005). In the frame cameras, the relationship of this sensor model to the perspective geometry used in photogrammetry should be determined. So, the camera calibration which is normaly undertaken by the manafacturer before selling the camera can be defined as the process of measuring the relationship of the perspective geometry and the actual frame camera geometry (Smith et al., 2007).

The new large format digital camera systems are geometrically complex systems because various groups of CCD arrays are shared to produce a number of images from different perspectives. These images are joined together from multiple lenses to produce a single image which is used for photogrammetry analysis. So, it is required to understand the geometry model of these cameras and analyze the relationship between the perspective geometry and the calibrated camera geometry. The geometric potential of digital cameras will affect the evaluation of the photogrammetric models (smith et al., 2005).

This paper provides an investigation into the large format digital camera geometry based on results achieved from two height flights flown over a test site in Germany as part of a DGPF project, resulting in two blocks with different Ground Sampling Distances (GSD), namely GSD 20cm and GSD 8cm. The high flight block (GSD=20cm) was flown with a forward overlap of 60%, while the low flight block (GSD=8cm) was flown with an 80% forward overlap. To allow for an inclusive comparison between all the cameras, the test flights were flown in similar conditions.

The quality of large format digital cameras is affected by many factors, ranging from the image measurement quality to the calibration of the integrated systems and the data processing strategies (Kruck, 2006). The strengths and weeknesses of these cameras can be measured by several parameters. One way of assessing this performance is comparing the digital camera to the traditional film based camera (Cramer et al., 2009). The photogrammetric and photographic issues should be taken into account when this comparison is performed. In order to investigate the quality of the large format digital camera performance (DMC and UltraCamX) in this paper, the geometric performance of these cameras was compared to the geometric performance of RMK TOP 15 camera.

AIM

The aim of this paper is to investigate the geometry strengths and weaknesses of large format aerial digital cameras. This will involve investigating the following objectives (Smith et al., 2006):

1. Understanding the geometry of large format aerial digital cameras.
2. Investigating an alternative camera calibration method.
3. Focusing on the analysis of geometric accuracy and sensor calibration.

The main aim of this paper is to derive the sensor specific strengths and maybe weaknesses, which are of relevance when later choosing a sensor for specific applications.

METHODOLOGY

The DGPF project provided a data set taken at two different altitudes over a targeted (pre-marked) test site in Vaihingen/Geramny. The methods used for the calibration model are as follows:

1. The Aerial Triangulation (AT) will be achieved without any calibration model. The results obtained from this scenario will be considered as benchmark results.
2. The Aerial Triangulation (AT) will be performed with the traditional self-calibration methods (1-12 additional parameters). These models were traditionally used with the large format film aerial cameras.
3. In this scenario, the systematic patterns in the image residuals should be identified and analyzed from the aerial triangulation through the individual sub-images and the whole image. The bundle adjustment will be re-computed based on the analysis of the systematic residual patterns. This

approach is based on analyzing the systematic errors of the high flown residuals and re-computing the bundle adjustment of the low flown images based on the residual corrections of the high flown images. This scenario will be investigated and considered a new approach. In this scenario, image residuals from all images will be explored in a sub-area of the image and the systematic patterns will be showed by the image residuals representing the sub-area. This could involve dividing the image into 25x25 sub-areas. Investigating residual plots of various numbers of subdivisions from one residual per CCD up to a high density of points per CCD, the 25x25 division seems to give a reasonably detailed distribution of residuals. The 25x25 division also appears to give a reasonable indication of any systematic patterns and therefore image coordinate correction (Smith et al., 2006).

Two softwares were used in this research; Leica LPS used for image observations and automatic tie point measurements, and the Institute of Photogrammetry and Geoinformation Leibniz University Hannover Program System (BLUH) analysis tools used to analyze the results.

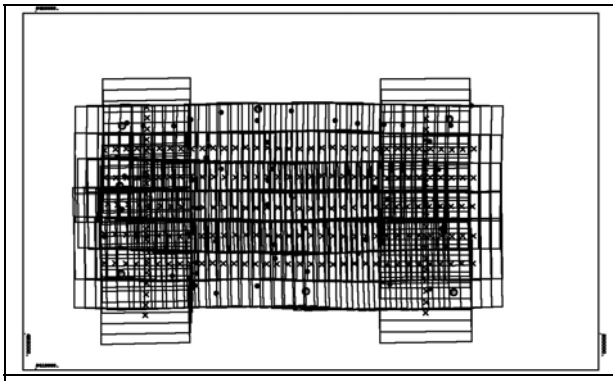

Figure 1: **UltraCamX-block with 8cm GSD**

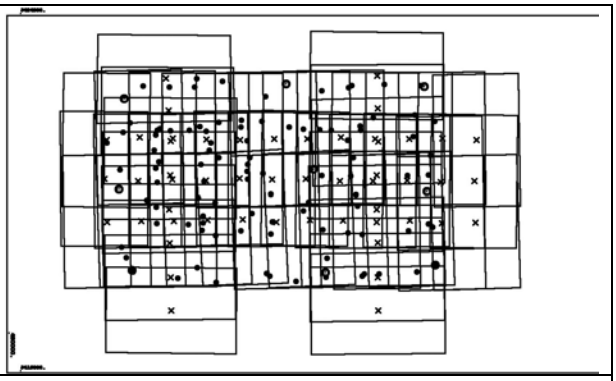

Figure 2: UltraCamX-block with 20cm GSD

TEST SITE AND DATA PROVIDED

The DGPF project consists of a data set taken at two different altitudes over a targeted (pre-marked) test site in Vaihingen/Geramny. The following block data sets were utilized within the test process. Figures 1 to 6 show the UltraCamX, the DMC and the RMK TOP 15 images blocks, respectively, taken at Ground Sample Distances (GSD) of 8 cm and 20 cm.

The actual pixel size of the object 8cm GSD-block UltraCamX is 8.6 cm and that of the 20cm GSD-block is 20.6 cm. The UltraCamX-block with 8cm GSD contains 215 images with a longitudinal coverage of 81% and 65% of congruent across, as well as 2 horizontal stripes (Fig. 1). The UltraCamX-block with 20cm GSD contains 52 images with a longitudinal coverage of 70% and 70% of congruent across, as well as 2 horizontal stripes (Fig. 2). In the 8cm GSD-block, the images contained on average 250 object points, while in the 20cm GSD-block, the object points were determined and the images in the middle 449 points abstained.

The actual pixel size of the object 8cm GSD-block DMC is 8.7 cm and that of the 20cm GSD-block is 21.6 cm. The DMC-block with 8cm GSD nominally contains 135 images with longitudinal and congruent across of 60%, and 2 stripes (Fig. 3). The DMC-block with 20cm GSD contains 60 images with longitudinal and congruent across of 60%, and also 2 stripes (Fig. 4). In the 8cm GSD-block, the images contained an average of 139 object points, while in the 20cm GSD-block the images contained an average of 177 object points.

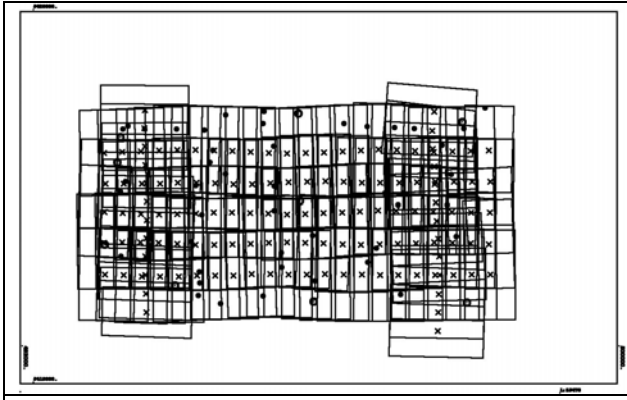

Figure 3: **DMC-block with 8cm GSD**

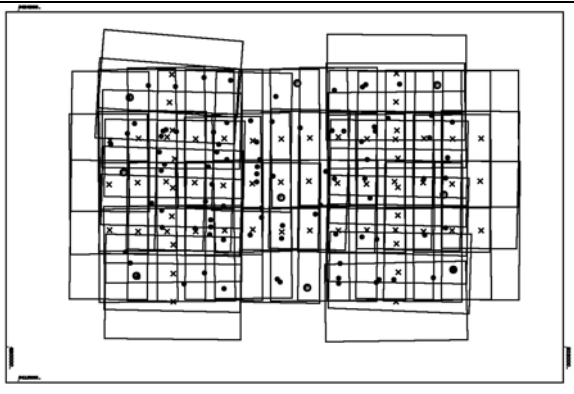

Figure 4: DMC-block with 20cm GSD

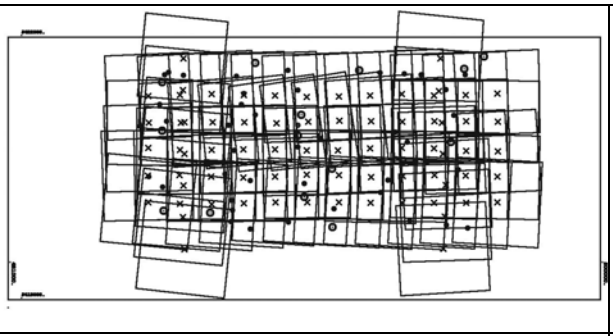

Figure 5: RMK-block with 8cm GSD

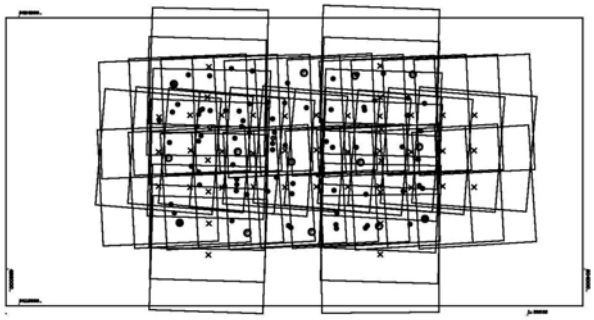

Figure 6: RMK-block with 20cm GSD

The RMK-block with 8cm GSD contains 74 images with a longitudinal and congruent across of 60%, and 2 horizontal stripes. 8cm GSD is matched to 14μm pixel size in the picture (Fig. 5). The RMK-block with 20cm GSD contains 47 images with longitudinal and congruent across of 60%, and 2 stripes (Fig. 6). 20cm GSD corresponds to 14μm pixel size in the image. In the 8cm GSD-block, the images contain on average 125 object points, while in the 20cm GSD-block, the images in the middle 235 points are included.

RESULTS AND DISCUSSION

General

It should be noted that the precision of the image observation relied on the radiometric image quality in both the high and low flights (Smith et al., 2007). The standard error used for the image observation was the σ_o value from a preliminary run of the aerial triangulation for a particular block being analyzed, typically 3-5μm. The numbers of control points and check points used were investigated on the benchmark results, making a reasonable assumption that this would be typical of all other triangulations.

RESULTS AND DISCUSSION-HIGH FLIGHT (GSD 20CM)

No Calibration Model-Benchmark Results

As camera calibration has already been performed by the vendors, the results were performed in the aerail triangulation without a calibration model and can be used as 'benchmark results' to which other results can be compared. The results are represented in Table 1.

The following figures indicate the image residuals of the observations in the image space for the results presented in Table 1.

Table 1: Results of high flight AT without any calibration model

Camera name/GCP/CP	Ground control points RMSE (m) of residuals			Ground check points RMSE (m) of residuals			Image coordinates RMSE (µm) of residuals		σo µm
	X	Y	Z	X	Y	Z	x	y	
Vexcel Imaging UltraCamX/9/99	0.052	0.061	0.146	0.075	0.083	0.163	0.79	0.85	1.00
Z/I Imaging DMC/9/95	0.031	0.040	0.178	0.045	0.078	0.184	1.45	1.28	1.90
Z/I Imaging RMK Top 15 film/14/82	0.093	0.061	0.130	0.112	0.116	0.154	4.75	4.29	5.90

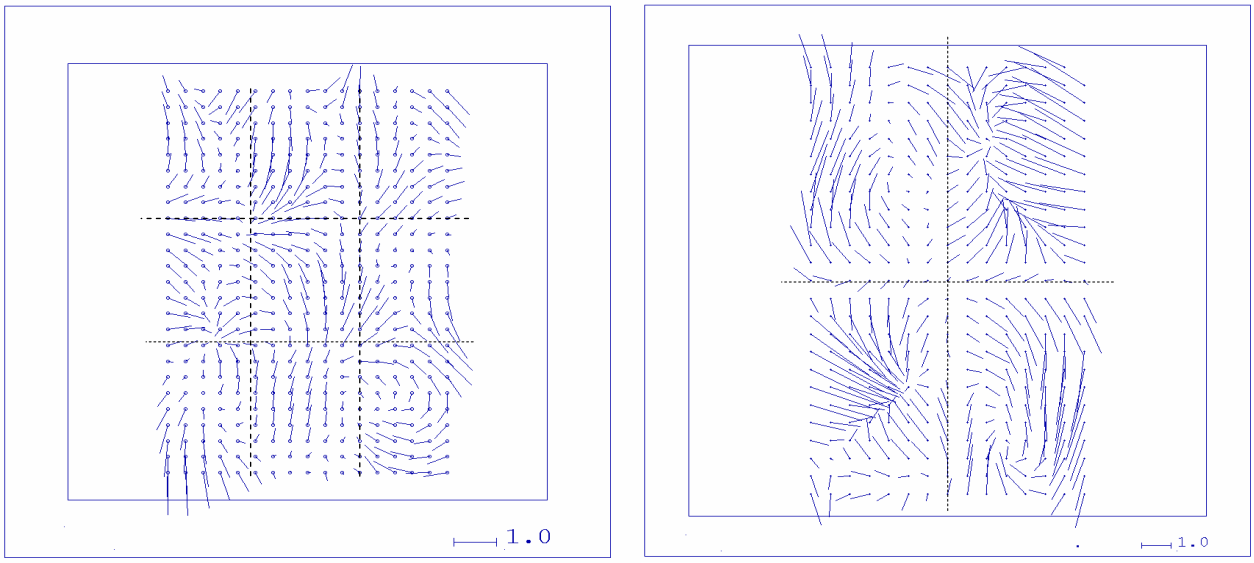

Figure 7: Mean image residuals in 25x25 sub-areas (UCX on the left and DMC on the right), results of AT without any calibration model (coordinates in µm, partitioning shows approximate boundaries of the CCD arrays)

On visual inspection of Figure 7 and Figure 8, there are overall identifiable systematic patterns in the whole image for all the three cameras, espicialy in Figure 8 for the film camera RMK Top 15. In Figure 7, there are small areas where systematic patterns can be identified, espicialy with DMC camera, some showing a relationship to the CCDs (9 CCDs for UltraCamX and 4 CCDs for DMC). As these residuals could come from a variety of sources and this is only a result from one block, these patterns may not be due to uncorrected systematic characteristics of camera/image geometry.

Results from Existing Self-calibration Models

A number of self-calibration models were tested to assess the most suitable for this type of imagery. The results presented here come from the traditional additional parameters in the BLUH software, and are considered the best results among existing self-calibration models based on the smallest image residuals and RMSE of ground and check points. The parameters of the self-calibration model are as follows (Smith et al., 2006):

c = principal distance

x_o, y_o = principal point position

a_1, a_2, a_3 = polynomial coefficients for radial lens distortions

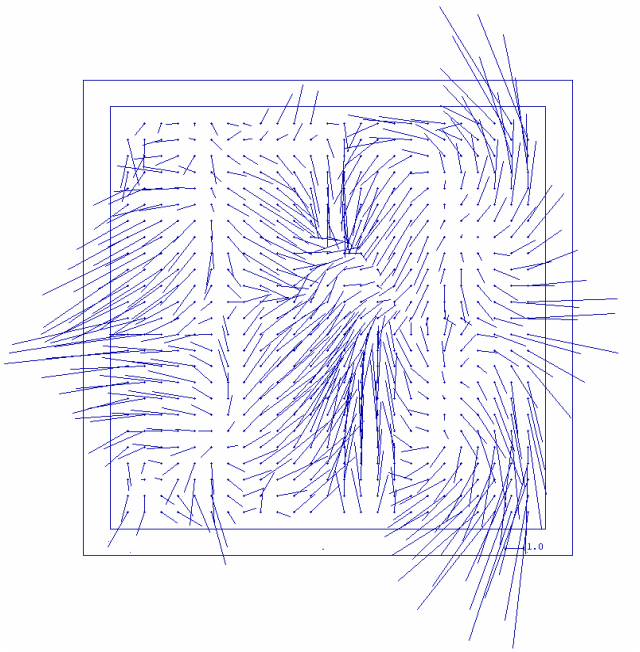

Figure 8: Mean image residuals in 25x25 sub-areas (Z/I Imaging RMK Top 15 film camera), results of AT without any calibration model (coordinates in µm, partitioning shows approximate boundaries of the CCD arrays)

Table 2: Results of high flight AT with the tradditional additonal parameters' self-calibration model

Camera name/GCP/CP	Ground control points RMSE (m) of residuals			Ground check points RMSE (m) of residuals			Image coordinates RMSE (µm) of residuals		σo µm
	X	Y	Z	X	Y	Z	x	y	
Vexcel Imaging UltraCamX/9/99	0.054	0.059	0.033	0.075	0.082	0.074	0.78	0.82	1.00
Z/I Imaging DMC/9/95	0.029	0.029	0.031	0.042	0.056	0.071	1.32	1.14	1.60
Z/I Imaging RMK Top 15 film/14/82	0.114	0.125	0.080	0.114	0.125	0.080	4.86	4.49	5.20

The results in Table 2 show a very significant improvement in Z coordinate compared to the benchmark values in Table 1 for the two cameras (UltraCamX and DMC) by adding the additional parameters of the self-calibration model. These additional parameters collect temperature influence on the board of the constant part panchromatic cameras and the radial distortion which is part of the cameras. So, a self-calibration with additional parameters is needed, particularly to improve the height accuracy.

Figure 9 and Figure 10 show an improvment on the pattern of the image residuals compared to the bench mark results in Figure 7 and Figure 8.

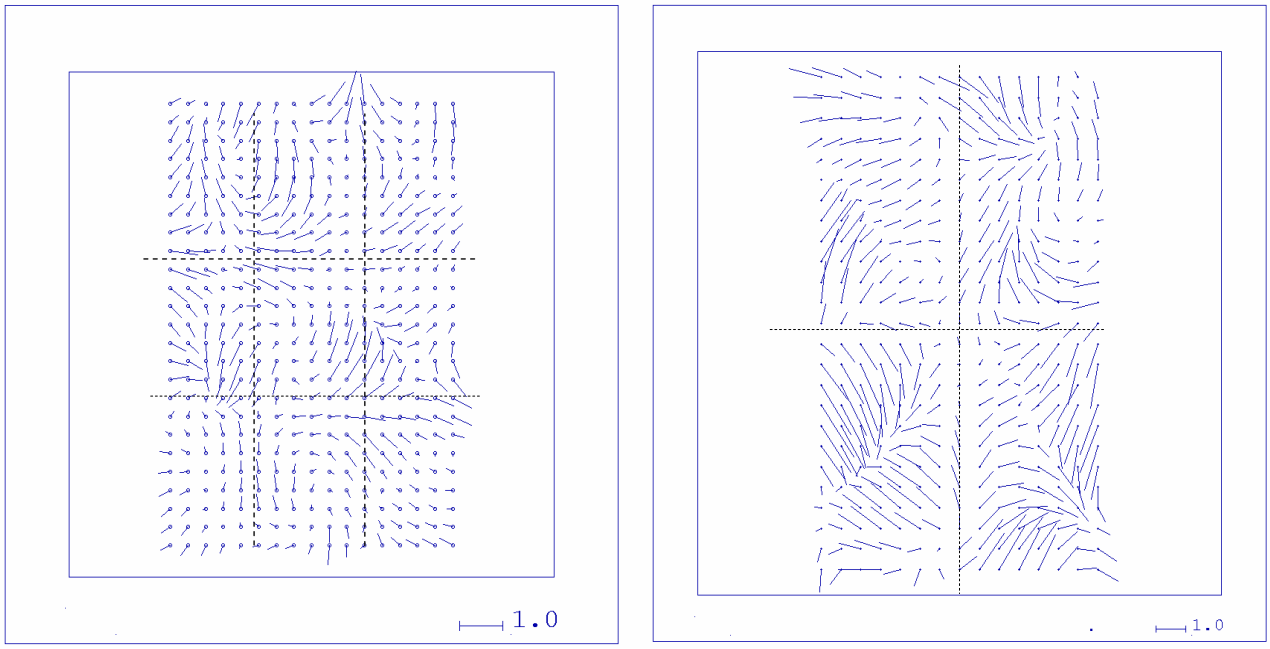

Figure 9: Mean image residuals in 25x25 sub-areas (UCX on the left and DMC on the right), results of AT with self-calibration model (coordinates in µm, partitioning shows approximate boundaries of the CCD arrays)

Table 3: Results of high flight AT with analysing the residuals in the aerial triangulation

Camera name/GCP/CP	Ground control points RMSE (m) of residuals			Ground check points RMSE (m) of residuals			Image coordinates RMSE (µm) of residuals		σo µm
	X	Y	Z	X	Y	Z	x	y	
Vexcel Imaging UltraCamX/9/99	0.053	0.058	0.125	0.074	0.082	0.143	0.76	0.79	0.90
Z/I Imaging DMC/9/95	0.036	0.032	0.129	0.043	0.066	0.149	1.40	1.19	1.70
Z/I Imaging RMK Top 15 film/14/82	0.093	0.066	0.099	0.114	0.118	0.125	4.57	4.06	5.30

Analysis of Aerial Triangulation Image Residuals

As the geometry of large format digital cameras is different from the traditional single cone/CCD camera, an analysis will be undertaken to try to identify any systematic patterns in the image residuals. This will enable alternative calibration procedures to be considered. The potential camera features which may cause variations from the traditional self-calibration model will be investigated through analysis of triangulation image residuals.

Applying the results shown in Figure 7 and Figure 8 to the measured image coordinates, as described in the methodology, gives the results in Table 3 using BLUH software without any self-calibrating model.

Applying the results shown in Figure 8 and Figure 9 to the measured image coordinates by identification and quantification of systematic residuals followed by the application to image coordinates and re-computation of

the bundle adjustment, as described in the methodology, gives the results in Table 3, Figure 11 and Figure 12 using BLUH software without any self-calibrating model. Figs. 11 and 12 show the mean image residuals of the observations for the sub-areas in the image. These figures indicate the image residuals for the results presented in Table 3. It appears, from visual inspection, that some of the systematic error patterns have been reduced. As the residuals of UCX camera are so small in Figure 11 (left Figure) compared to Figure 7 (left figure), the solution appears to have reduced some of the residual pattern, although the residuals in the DMC camera seem to still have some relatively large residuals.

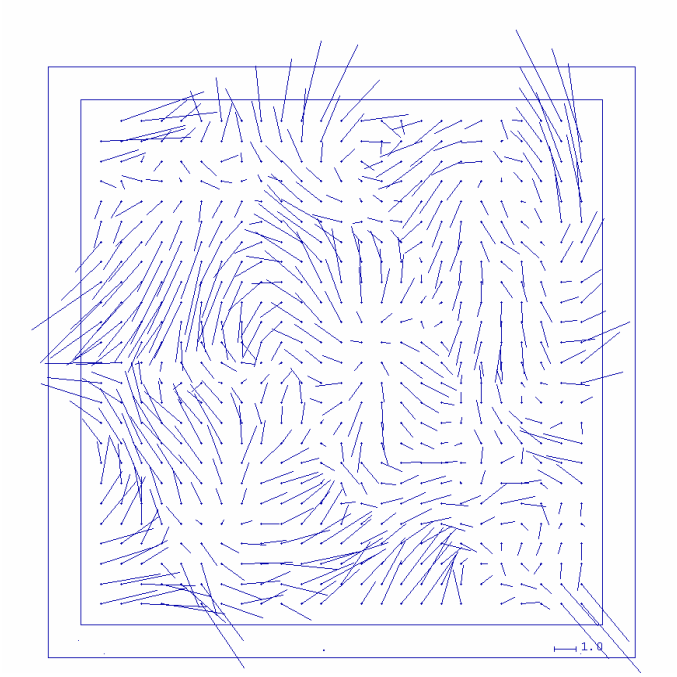

Figure 10: Mean image residuals in 25x25 sub-areas (Z/I Imaging RMK Top 15), results of AT with self-calibration model (coordinates in µm, partitioning shows approximate boundaries of the CCD arrays)

Summary of High Flight Results

Table 4 shows that the results of the ground control RMSE are significantly better than the ground control check point RMSE values. The ground control RMSE values are influenced by the standard errors of the image coordinates and the ground control. The standard error of ±0.05m for the ground control was provided and the standard error used for the image observation was the σ_o value from a preliminary run of the aerial triangulation for a particular block being analyzed, typically 3-5µm. Table 4 also shows that, in general, a significant improvement has been obtained from the self-calibration model in the Z coordinate for the check control points. The self-calibration model is probably corrected for some environmental effects. The adding residuals approach has slightly improved the RMSE of the image residuals, with a minimal improvement of the ground and check control RMSE.

RESULTS AND DISCUSSION - LOW FLIGHT (GSD 8CM)

A similar process used for analyzing the high flown images has been used to assess the low flown images except for the adding residuals approach, and the high flown residual correction has been used in the low flown computation. This correction was used because

the ideal scenario would be to compute the residual corrections from a block of triangulations and then assuming this was a systematic pattern for all images, this would be applied until a new correction was computed. It is important to note that the results from the aerial triangulation in the BLUH model were obtained using the cross strips in the low flight.

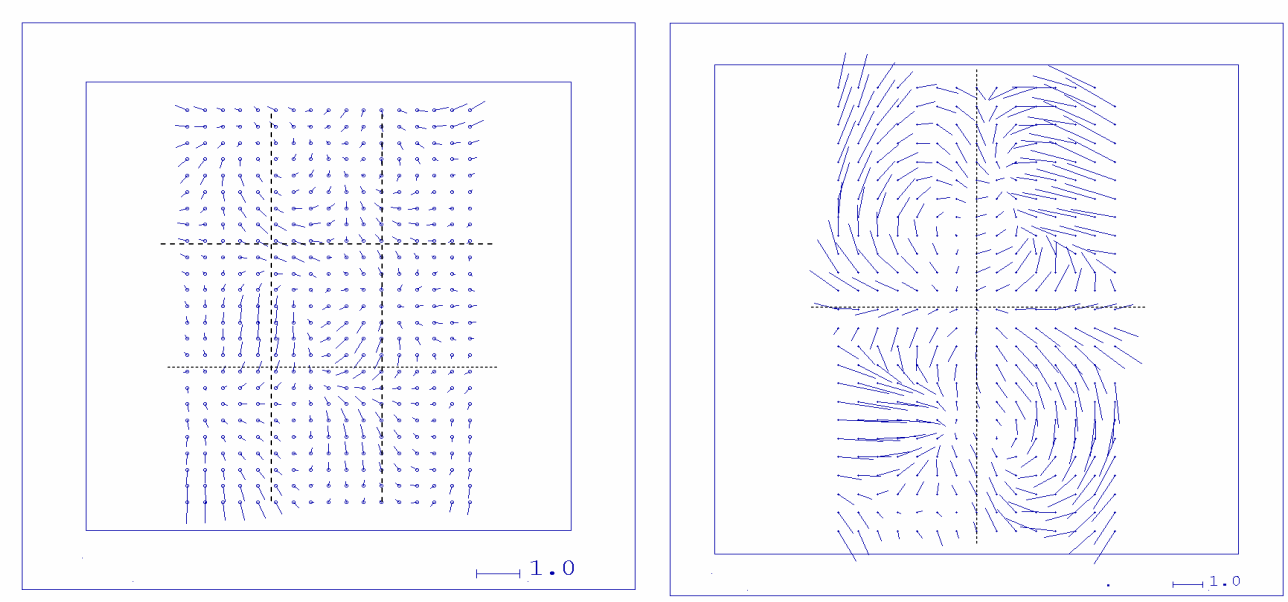

Figure 11: Mean image residuals in 25x25 sub-areas (UCX on the left and DMC on the right), results of AT with adding the residuals' approach (coordinates in µm, partitioning shows approximate boundaries of the CCD arrays)

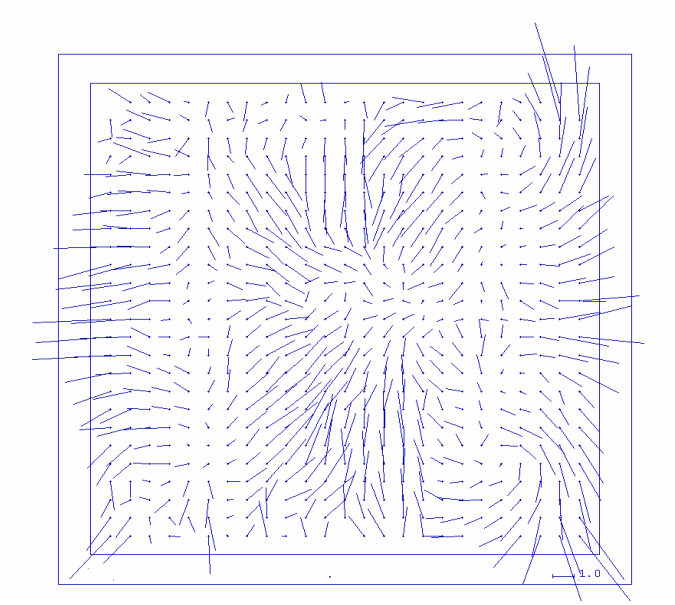

Figure 12: Mean image residuals in 25x25 sub-areas (Z/I Imaging RMK Top 15), results of AT with adding the residuals' approach (coordinates in µm, partitioning shows approximate boundaries of the CCD arrays)

Table 4: Summary of high flight results

Camera name/GCP/CP	Calibration Model	Ground control points RMSE (m) of residuals			Ground check points RMSE (m) of residuals			Image coordinates RMSE (µm) of residuals		σo µm
		X	Y	Z	X	Y	Z	x	y	
Vexcel Imaging UltraCamX/9/99	No	0.052	0.061	0.146	0.075	0.083	0.163	0.79	0.85	1.00
	Self Calibration	0.054	0.059	0.033	0.075	0.082	0.074	0.78	0.82	1.00
	residuals from high flight	0.053	0.058	0.125	0.074	0.082	0.143	0.76	0.79	0.90
Z/I Imaging DMC/9/95	No	0.031	0.040	0.178	0.045	0.078	0.184	1.45	1.28	1.90
	Self Calibration	0.029	0.029	0.031	0.042	0.056	0.071	1.32	1.14	1.60
	residuals from high flight	0.036	0.032	0.129	0.043	0.066	0.149	1.40	1.19	1.70
Z/I Imaging RMK Top 15 film/14/40	No	0.093	0.061	0.130	0.112	0.116	0.154	4.75	4.29	5.90
	Self Calibration	0.114	0.125	0.080	0.114	0.125	0.080	4.86	4.49	5.20
	residuals from high flight	0.093	0.066	0.099	0.114	0.118	0.125	4.57	4.06	5.30

Table 5: Results of low flight AT without self-calibration model

Camera name/GCP/CP	Ground control points RMSE (m) of residuals			Ground check points RMSE (m) of residuals			Image coordinates RMSE (µm) of residuals		σo µm
	X	Y	Z	X	Y	Z	x	y	
Vexcel Imaging UltraCamX/9/99	0.029	0.035	0.030	0.044	0.053	0.054	0.75	0.84	0.90
Z/I Imaging DMC/9/95	0.013	0.023	0.044	0.022	0.037	0.077	3.16	2.45	3.30
Z/I Imaging RMK Top 15 film/14/82	0.018	0.031	0.108	0.020	0.040	0.152	4.19	4.17	4.60

No Calibration Model - Benchmark Results

It is interesting to note that the image coordinate RMSE values are larger than for the high flight indicating a less quality of measurement and/or image quality. In addition, the difference in the image residuals could have been also influenced by the difference in the number of tie points between the low flight and high flight. The RMSE values of the ground check points are good in X and Y but the Z value for the check points is a little large compared with the ground control Z value. Figure 13 and Figure 14 show the image residuals of the observation in the image space for the results presented in Table 5. If there is any systematic pattern in the images, then there should be a similarity with the pattern of residuals in Figure 7 and Figure 8. By visual inspection, there is some similarity between the patterns of residuals for UCX camera in Figure 7 and Figure 13.

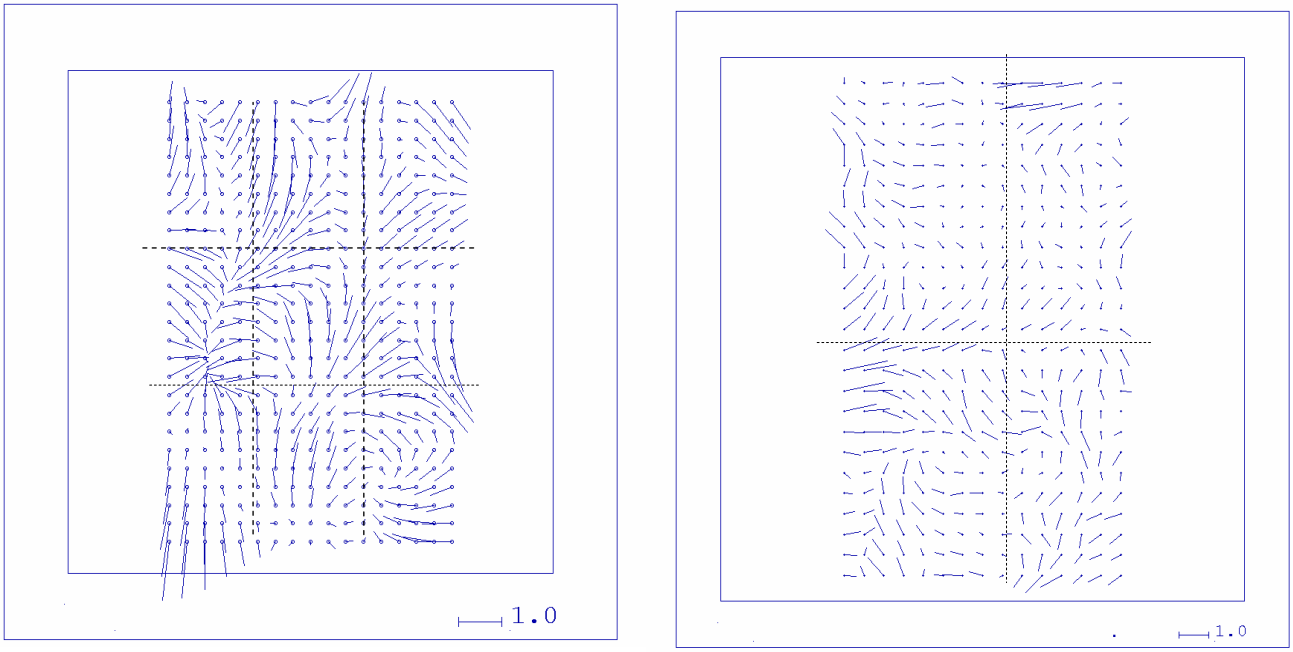

Figure 13: Mean image residuals in 24x24 sub-areas (UCX on the left and DMC on the right), results of AT without calibration model(coordinates in µm, partitioning shows approximate boundaries of the CCD arrays)

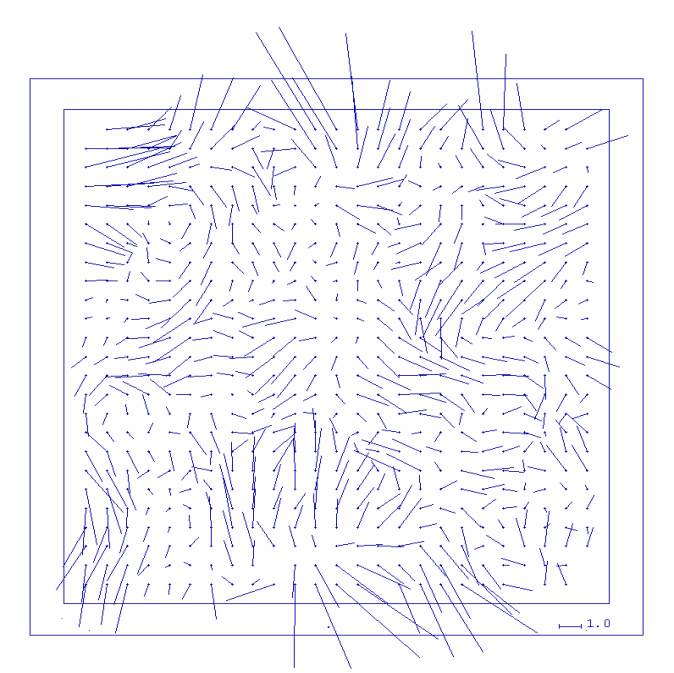

Figure 14: **Mean image residuals in 25x25 sub-areas (Z/I Imaging RMK Top 15), results of AT without calibration model (coordinates in µm, partitioning shows approximate boundaries of the CCD arrays)**

Table 6: Results of low flight AT with self-calibration model

Camera name/GCP/CP	Ground control points RMSE (m) of residuals			Ground check points RMSE (m) of residuals			Image coordinates RMSE (µm) of residuals		σo µm
	X	Y	Z	X	Y	Z	x	y	
Vexcel Imaging UltraCamX/9/99	0.028	0.033	0.029	0.042	0.050	0.037	0.73	0.80	0.90
Z/I Imaging DMC/9/95	0.014	0.019	0.013	0.023	0.029	0.033	3.07	2.37	3.20
Z/I Imaging RMK Top 15 film/14/82	0.016	0.026	0.038	0.020	0.033	0.049	4.23	4.21	4.30

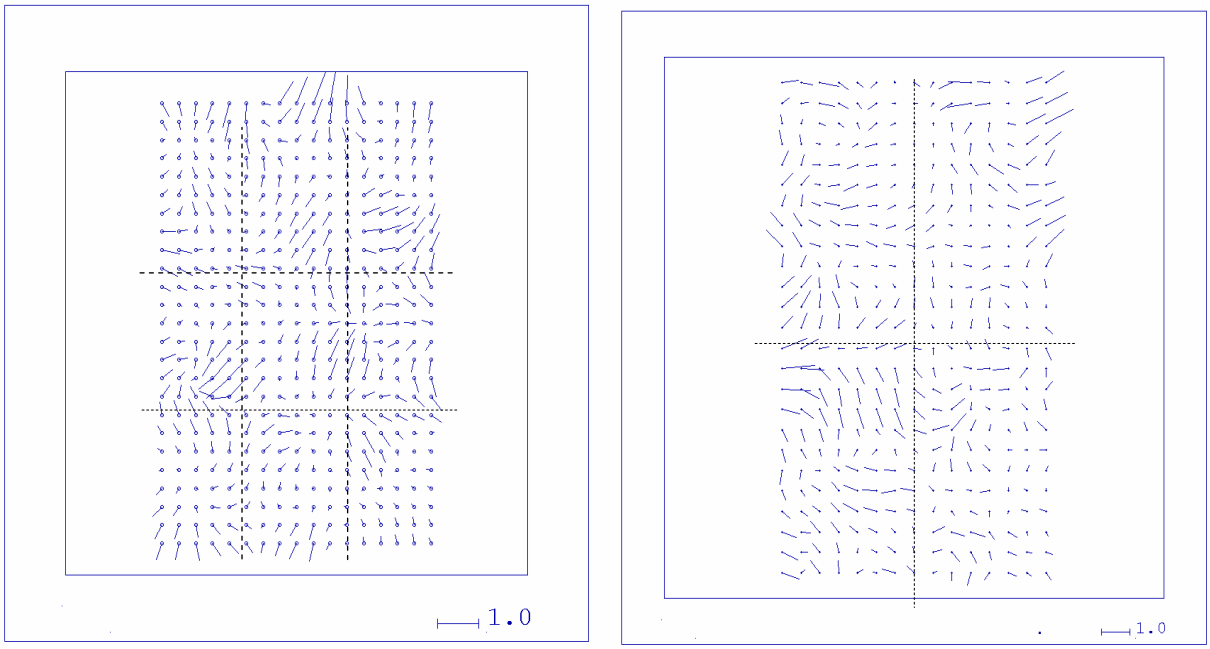

Figure 15: Mean image residuals in 25x25 sub-areas (UCX on the left and DMC on the right), results of AT with self-calibration model (coordinates in µm, partitioning shows approximate boundaries of the CCD arrays)

The Results from Existing Self-calibration

A number of self-calibration models were tested using BLUH software to assess the most suitable for this type of imagery. The results presented here come from BLUH and are considered the 'best' results from existing self-calibration models based on the smallest image residuals and RMSE of ground and check points. The parameters of the self-calibration model are as follows:

c = principal distance

x_o, y_o = principal point position

a_1, a_2, a_3 = polynomial coefficients for radial lens distortions

Figure 15 and Figure 16 indicate the image residuals of the observations in the image space for the results presented in Table 6. There is an improvment in the pattern of residuals compared to those shown in Figure 13 and Figure 14.

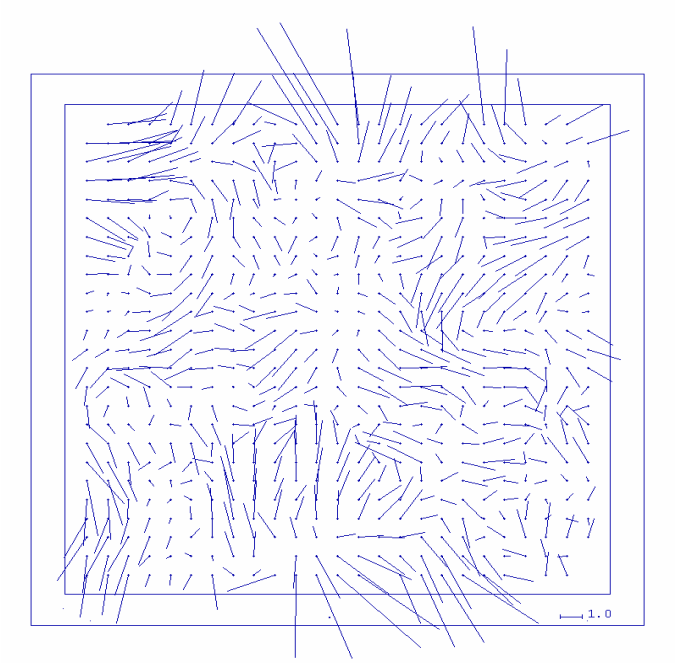

Figure 16: Mean image residuals in 25x25 sub-areas (Z/I Imaging RMK Top 15), results of AT with self-calibration model (coordinates in µm, partitioning shows approximate boundaries of the CCD arrays)

Table 7: Results of AT with analyzing the residuals in the aerial triangulation

Camera name/GCP/CP	Ground control points RMSE (m) of residuals			Ground check points RMSE (m) of residuals			Image coordinates RMSE (µm) of residuals		σo µm
	X	Y	Z	X	Y	Z	x	y	
Vexcel Imaging UltraCamX/9/99	0.028	0.034	0.027	0.044	0.052	0.042	0.72	0.78	0.90
Z/I Imaging DMC/9/95	0.036	0.032	0.129	0.022	0.029	0.041	3.15	2.44	3.20
Z/I Imaging RMK Top 15 film/14/82	0.019	0.029	0.098	0.017	0.030	0.106	4.19	4.17	4.50

Analysis of Aerial Triangulation Image Residuals from High Flight

In this trial, the image coordinate corrections that have been applied are the values computed from the high flown block. Figure 17 and Figure 18 indicate the image residuals of the observations in the image space for the results presented in Table 7. It appears, from visual inspection, that some of the patterns have been reduced and there is a significant improvment in the image coordinates compared to those in Figures 13 and 14.

Summary of Low Flight Results

Table 8 shows again small RMSE values for ground control points as identified in the high flown trials. It also shows an improvement in applying a traditional single lens self-calibration model technique, espicialy in the Z coordinate. This has really reduced relatively

significantly the x and y image residuals and the Z RMSE values for the check points compared to the bench mark values. The residual corrections from the high flown block have been used.

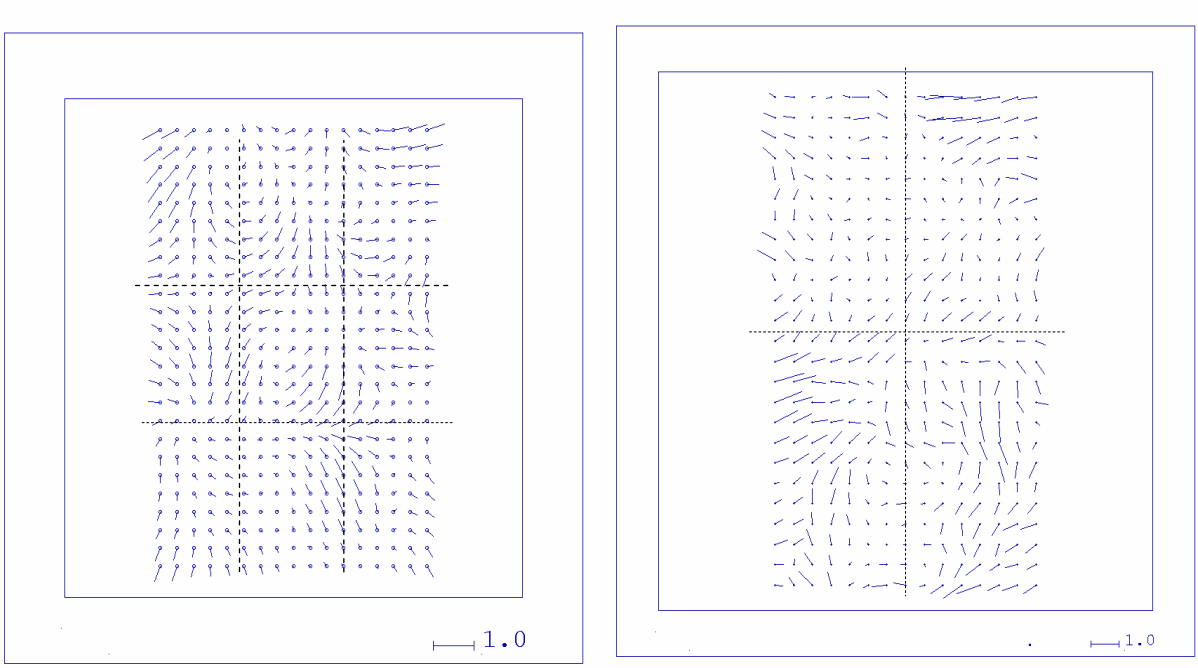

Figure 17: **Mean image residuals in 25x25 sub-areas (UCX on the left and DMC on the right), results of AT with adding the high flight residuals (coordinates in µm, partitioning shows approximate boundaries of the CCD arrays)**

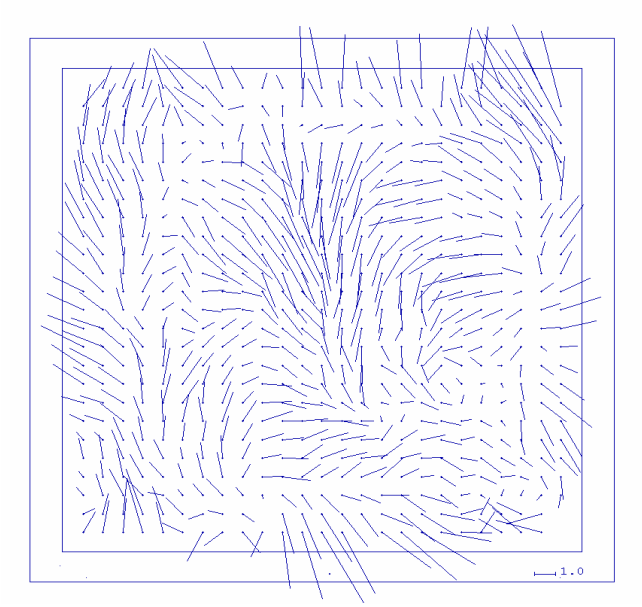

Figure 18: Mean image residuals in 25x25 sub-areas (Z/I Imaging RMK Top 15), results of AT with the adding residuals approach (coordinates in µm, partitioning shows approximate boundaries of the CCD arrays)

Table 8: Summary of low flight results

Camera Name/GCP/CP	Calibration Model	Ground control points RMSE (m) of residuals			Ground check points RMSE (m) of residuals			Image coordinates RMSE (µm) of residuals		σo µm
		X	Y	Z	X	Y	Z	x	y	
Vexcel Imaging UltraCamX/9/99	No	0.029	0.035	0.030	0.044	0.053	0.054	0.75	0.84	0.90
	Self Calibration	0.028	0.033	0.029	0.042	0.050	0.037	0.73	0.80	0.90
	residuals from high flight	0.028	0.034	0.027	0.044	0.052	0.042	0.72	0.78	0.90
Z/I Imaging DMC/9/95	No	0.013	0.023	0.044	0.22	0.037	0.077	3.16	2.45	3.30
	Self Calibration	0.014	0.019	0.013	0.023	0.029	0.033	3.07	2.37	3.20
	residuals from high flight	0.036	0.032	0.129	0.022	0.029	0.041	3.15	2.44	3.20
Z/I Imaging RMK Top 15 film/14/40	No	0.018	0.031	0.108	0.020	0.040	0.152	4.19	4.17	4.60
	Self Calibration	0.016	0.026	0.038	0.020	0.033	0.049	4.23	4.21	4.30
	residuals from high flight	0.019	0.029	0.098	0.017	0.030	0.106	4.19	4.17	4.50

CONCLUSIONS

Both flights show that ground control RMSE values are significantly better than the ground control check point RMSE values. This is rather unexpected as we are not conscious of using any incorrect weighing to the control.

Many systematic patterns were visually detected in small areas of the image. The new approach has made a small improvement of the results. This new calibration approach for the low flight has been mostly useful in improving the RMSE in Z and decreasing image residuals. But, the method was less successful at improving the high flown results.

More tests are necessary with a number of blocks to fully understand the residual patterns that are being created not only within the images of a block but also among blocks.

The existing self-calibration methods and the adding residuals approach have made a significant improvement of the results. The adding residuals approach for the low flight has been particularly beneficial in improving the RMSE in Z and reducing image residuals. However, the method was less successful at improving the high flown results used to compute the correction for the low flown blocks.

The new approach has showed that it needs further investigation to fully assess its capabilities. It is surprising that this new approach did not make as much improvement with the high flown block, which was used to calculate the correction, as it did with the low flown block. Subjects such as optimum subdivision of the image would also need to form part of this study. Similar trials and analyses are being carried out using both the high and the low flown flights altogether.

All investigated systems needed a block triangulation with self-calibration by additional parameters or any suitable approach for self-calibration.

To the cameras adjusted by the new approach described in this paper, the results are improved.

REFERENCES

Cramer, M. 2005. Digital Airborne Cameras-Status and Future. ISPRS Hannover Workshop on High Resolution Earth Imaging for Geospatial Information Proceedings, Volume XXXVI Part I/W3, ISSN No. 1682-1777.

Cramer, M. and Haala, Norbert. 2009. DGPF Project: Evaluation of Digital Photogrammetric Aerial Based Imaging Systems – Overview and Results from the Pilot Centre. ISPRS Hannover Workshop on High Resolution Earth Imaging for Geospatial Information Proceedings, Volume XXXVIII-1-4-7_W5.

Gruber, M. and Ladstädler, R. 2006. Geometric Issues of the Digital Large Format Aerial Camera UltraCamD. International Calibration and Orientation Workshop, EuroCOW 2006. January 2006, Castelldefels, Spain. EuroSDR Commission I and ISPRS Working Group 1/3.

Jacobsen, K. 2009. DGPF-Projekt: Evaluierung Digitaler Photogrammetrischer Luftbildkamerasysteme– Auswerteteam Geometrie. DGPF Tagungsband.

Kruck, E. 2006. Simultaneous Calibration of Digital Aerial Survey Cameras. International Calibration and Orientation Workshop, EuroCOW 2006. January 2006, Castelldefels, Spain. EuroSDR Commission I and ISPRS Working Group 1/3.

Smith, M. J., Kokkas, N. and Qtaishat, K. S. 2007. Investigation into Self-Calibration Methods for the Vexcel UltraCam D Digital Aerial Camera. In: ISPRS Hannover Workshop on High Resolution Earth Imaging for Geospatial Information, 29 May - 1 June, 6.

Smith, M.J., Qtaishat, K.S., Park, D.W.G. and Jamieson, A. 2006. IMU and Digital Aerial Camera Misalignment Calibration. In: EuroCOW 2006. International Calibration and Orientation Workshop, 25-27 January 2006, Castelldefels, Spain.

Smith, M.J., Qtaishat, K.S., Park, D.W.G. and Jamieson, A. 2005. Initial Results from the Vexcel UltraCam Digital Aerial Camera. In: Heipke, C., Jacobson, K. and Gerke, M., eds. ISPRS Hannover Workshop on High-Resolution Earth Imaging for Geospatial Information, Hannover, Germany. ISPRS, International Society for Photogrammetry and Remote Sensing, v XXXVI, Co I WGI/1, 6.